

Hole drift velocity in germanium

L. Reggiani, C. Canali, F. Nava, and G. Ottaviani

Istituto di Fisica, Università di Modena, via Università 4, 41100 Modena, Italy

(Received 14 April 1976)

Drift velocity for holes in high-purity Ge ($|N_D - N_A| < 10^{11} \text{ cm}^{-3}$) has been analyzed for a wide range of temperatures $8 \leq T \leq 220^\circ\text{K}$ and fields $1 \leq E \leq 10^4 \text{ V/cm}$ applied parallel to $\langle 100 \rangle$, $\langle 110 \rangle$, and $\langle 111 \rangle$ crystallographic directions. Experiments are carried out with the time-of-flight technique and theory uses a Monte Carlo method. The physical model includes warping and nonparabolic effect of the heavy-hole band, as well as acoustic and non-polar optical scattering mechanisms. In the case of the acoustic scattering mechanism, energy dissipation and the correct phonon population have been included.

I. INTRODUCTION

This work presents experimental and theoretical investigations of the hole-drift velocity v_d in high-purity Ge, as a function of temperature and electric field applied parallel to different crystallographic directions.¹

Although several papers exist in the literature, they generally concentrate on particular aspects of the subject, and no exhaustive paper exists. For instance, Ohmic mobility is dealt with in Refs. 2–7, while the non-Ohmic region, with particular emphasis on the hot-carrier distribution function, is investigated in Refs. 8–10. Mobility, noise temperature, and diffusivity of hot holes are reported in Ref. 11 and, recently, the anisotropy of v_d at high fields has been measured and interpreted at 77°K on the basis of the warping of the heavy-hole band.¹²

The aim of this paper is to demonstrate that a wide range of experimental data can be interpreted within the framework of a well-accepted theoretical model. New measurements of v_d are performed in the temperature range $8 \leq T \leq 220^\circ\text{K}$, and for electric fields between 1 and 10^4 V/cm applied parallel to the crystallographic directions $\langle 111 \rangle$ and $\langle 110 \rangle$; these results complete a previous experimental investigation.¹³ The theoretical analysis makes use of the Monte Carlo technique in solving the Boltzmann equation. Its main objectives are (i) to interpret anisotropic effects over the whole temperature range; (ii) to analyze nonparabolicity effects, with particular reference to the highest fields and the saturation region of v_d ; and (iii) to introduce acoustic dissipation into the theory.

Section II describes the experimental technique and reports the data. The theoretical approach is given in Sec. III. In Sec. IV the comparison between theory and experiments is reported and discussed.

II. EXPERIMENTAL TECHNIQUE AND RESULTS

The experimental procedure makes use of the time-of-flight technique. This technique has been extensively used and is discussed in other papers.^{14,15}

The samples used in this experiment were $n^+ - i - p^+$ diodes made of high-purity germanium supplied by General Electric and Lawrence Berkeley Laboratory. The n^+ and p^+ contacts were formed by solid-phase epitaxy at 350°C , using Al and Sb, respectively. The low temperature involved in such a process prevents contaminations of the material.¹⁶

Several samples were obtained from the same ingot, being cut perpendicular to the crystallographic axes $\langle 111 \rangle$, $\langle 110 \rangle$, $\langle 100 \rangle$ with an accuracy of $\pm 1^\circ$.

The samples varied in thickness from 220 to $790 \mu\text{m}$ and had a useful area of about 10 mm^2 approximately at the center of 1-cm^2 disks. Their characteristics are reported in Table I.

A detailed analysis of the experimental errors has been reported in Ref. 17. In the present case, the total experimental error of v_d is $\pm 5\%$ and derives from the measurements of sample thickness and charge-carrier transit time.

The samples were mounted in such a way as to minimize thermal gradients. To avoid heating effects, we used a pulsed-bias voltage at low repetition rate (100 Hz). The temperature was measured with a germanium resistor in the range $8\text{--}77^\circ\text{K}$, and with a thermocouple in the range $77\text{--}220^\circ\text{K}$.

The error in evaluating the temperature of the samples was 0.3°K in the former case and 1°K in the latter.

The effects of the thermalization process of the highly excited carriers produced by the 30-keV primary electrons was checked using samples of different thicknesses. The same drift velocity

TABLE I. Characteristics of the samples used in drift velocity measurements. The material has been supplied by General Electric and Lawrence Berkley Laboratory.

Sample	Ingot No.	Thickness (in μm)	Crystal axis	Net-impurity conc. (in cm^{-3})	Type	Dislocation density (in cm^{-2})
1	A	220	$\langle 111 \rangle$	7.8×10^{10}	p/π	1000
2	A	420	$\langle 111 \rangle$	7.8×10^{10}	p/π	1000
3	B	280	$\langle 111 \rangle$	2×10^{10}	p	1500
4	B	530	$\langle 111 \rangle$	2×10^{10}	p	1500
5	C	260	$\langle 111 \rangle$	1×10^{10}	n	1500
6	C	340	$\langle 111 \rangle$	1×10^{10}	n	1500
7	C	470	$\langle 111 \rangle$	1×10^{10}	n	1500
8	C	220	$\langle 100 \rangle$	1×10^{10}	n	1500
9	C	420	$\langle 100 \rangle$	1×10^{10}	n	1500
10	C	480	$\langle 100 \rangle$	1×10^{10}	n	1500
11	C	520	$\langle 100 \rangle$	1×10^{10}	n	1500
12	D	300	$\langle 111 \rangle$	$< 10^{10}$	Mixed	$10^3 - 10^4$
13	D	715	$\langle 111 \rangle$	$< 10^{10}$	Mixed	$10^3 - 10^4$
14	E	270	$\langle 111 \rangle$	9×10^9	p	1000
15	E	315	$\langle 111 \rangle$	9×10^9	p	1000
16	E	470	$\langle 110 \rangle$	9×10^9	p	1000
17	E	640	$\langle 110 \rangle$	9×10^9	p	1000
18	E	775	$\langle 110 \rangle$	9×10^9	p	1000
19	E	255	$\langle 100 \rangle$	9×10^9	p	1000
20	E	460	$\langle 100 \rangle$	9×10^9	p	1000
21	E	735	$\langle 100 \rangle$	9×10^9	p	1000
22	F	295	$\langle 111 \rangle$	1.1×10^{10}	Mixed	5×10^3
23	F	790	$\langle 111 \rangle$	1.1×10^{10}	Mixed	5×10^3
24	G	285	$\langle 100 \rangle$	$(1-2) \times 10^{10}$	Mixed	1500
25	G	370	$\langle 100 \rangle$	$(1-2) \times 10^{10}$	Mixed	1500
26	G	630	$\langle 100 \rangle$	$(1-2) \times 10^{10}$	Mixed	1500

versus electric field obtained in all the samples over the whole temperature range examined ensures that the thermalization time is much less than the minimum measured transit time.

These experimental results also support the view that the transit time is much greater than the time necessary for the carriers to reach a steady-state condition.

On changing the density of the carrier crossing the sample from 10^{12} to 10^{14} cm^{-3} , no effect on the transit time was observed. Such a result seems to indicate that, at our concentration, the effect of hole-hole scattering on drift velocity is negligible.

Experimental results relating to hole-drift velocity for temperatures between 8 and 220 °K, and electric fields ranging between 1 and 10^4 V/cm applied in the $\langle 111 \rangle$ direction are shown in Fig. 1. For clarity, the data are reported as a solid line, each line representing the average value of several determinations of drift velocity performed in different samples.

In order to display the anisotropy effect, the

drift velocities obtained at the same temperatures as in Fig. 1, with the electric field applied parallel to the $\langle 111 \rangle$ and $\langle 100 \rangle$ axes, are shown in Fig. 2 together with theoretical results. The data ob-

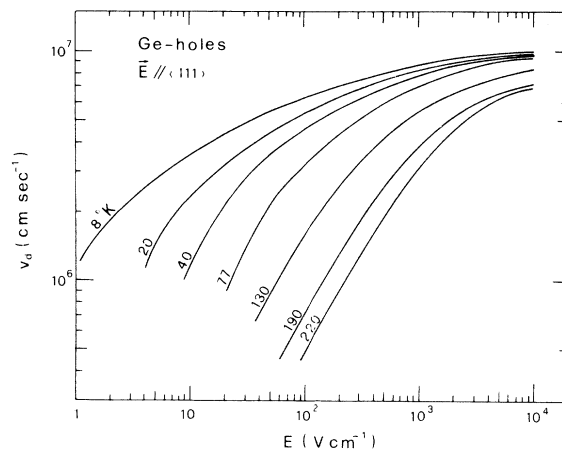


FIG. 1. Experimental hole-drift velocity as a function of electric field applied parallel to a $\langle 111 \rangle$ direction at different temperatures.

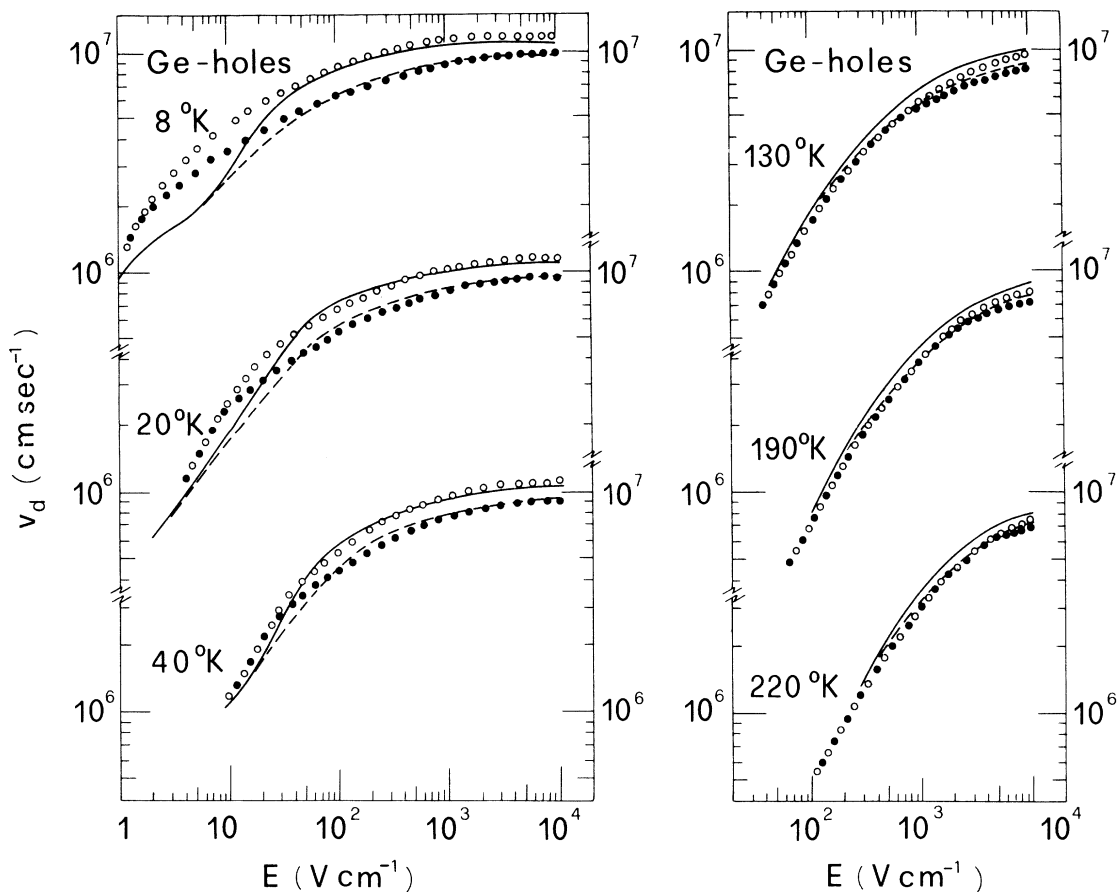


FIG. 2. Hole-drift velocity v_d as a function of electric field E at the different temperatures indicated. Open and closed circles refer to experimental data obtained with the field parallel to $\langle 100 \rangle$ and $\langle 111 \rangle$ directions, respectively. Continuous and dashed lines indicate the theoretical results obtained for the $\langle 100 \rangle$ and $\langle 111 \rangle$ directions, respectively.

tained by applying the field parallel to the three high-symmetry directions $\langle 111 \rangle$, $\langle 110 \rangle$, and $\langle 100 \rangle$ at $T = 77^\circ\text{K}$ are given in Fig. 3, together with theoretical results.

The main features of the present data can be summarized as follows: (i) At the lowest electric field applied, the experimental values reach the Ohmic region only at $T \geq 77^\circ\text{K}$, while at lower temperatures they approach the Ohmic region without actually reaching it. (ii) In the non-Ohmic region the hole-drift velocity exhibits an anisotropic behavior, with higher values for v_d in the $\langle 100 \rangle$ direction than in the $\langle 111 \rangle$ direction. Anisotropy increases as the field increases until, at the highest field values ($E \approx 10^4$ V/cm), it remains nearly constant. Anisotropy is best demonstrated by lowering the temperature, its maximum effect, with a $v_{d100}/v_{d111} - 1 \approx 34\%$, being observed at 8°K for $E \approx 300$ V/cm. At 77°K measurements, made with E parallel to the $\langle 110 \rangle$ direction, showed that

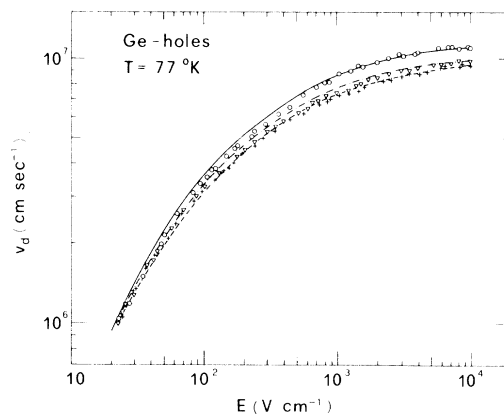


FIG. 3. Hole-drift velocity v_d as a function of electric field E at 77°K . \circ refers to $E \parallel \langle 100 \rangle$, ∇ refers to $E \parallel \langle 110 \rangle$, $+$ refers to $E \parallel \langle 111 \rangle$. Continuous, dot-dashed, and dashed lines refer to theoretical results for $E \parallel \langle 100 \rangle$, $E \parallel \langle 110 \rangle$, and $E \parallel \langle 111 \rangle$, respectively.

v_{d100} is consistently slightly higher than v_{d111} , with a maximum effect $v_{d110}/v_{d111} - 1 \approx 8\%$ at the highest fields. (iii) At the highest fields a net defined saturation value of v_d in the $\langle 100 \rangle$ direction shows up at temperatures of 8, 20, and 40 °K. In the $\langle 111 \rangle$ direction at the same temperatures, this effect does not appear so evidently.

A. Ohmic mobility and comparison with other data

In Fig. 4, the experimental data of Ohmic mobility, obtained by several authors with ionized impurity concentrations ranging between about 10^{11} and 10^{13} cm $^{-3}$, are reported as a function of temperature, together with present mobility values obtained for the v_d/E ratio calculated at the lowest applied fields. The different data agree well down to temperatures of about 20 °K. Below this temperature, the present data and those of De Laet *et al.*¹⁸ give higher mobility values than those of Brown and Bray.⁴ A slight effect of ionized impurity scattering in the data of Brown and Bray⁴ seems to account for this discrepancy.

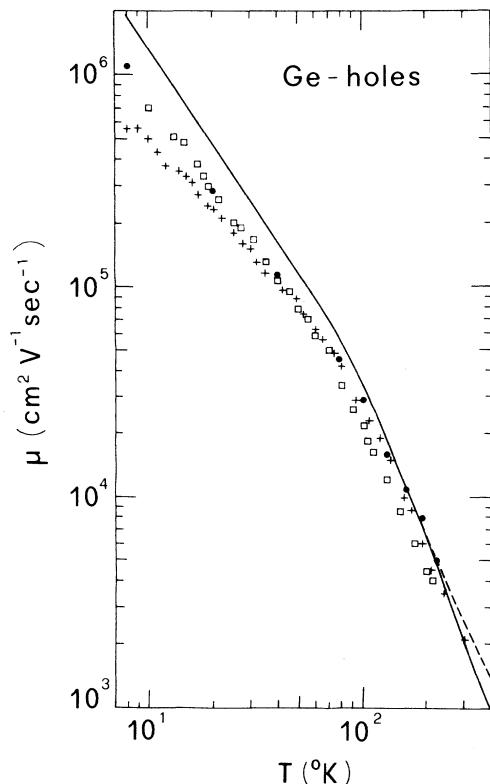


FIG. 4. Mobility μ of holes in Ge as a function of temperature. The dashed and continuous lines show the respective Monte Carlo theoretical results in the parabolic case and in the case where nonparabolic effect are taken into account. +, Brown and Bray (Ref. 4); ○, Ottaviani *et al.* (Ref. 13); □, De Laet *et al.* (Ref. 18).

Our data on the field dependence of v_d agree with the results of Ref. 19 at 77 °K and for E parallel to the $\langle 111 \rangle$ direction; however, the scarcity of available data in literature prevents more detailed comparison.

III. THEORETICAL APPROACH

A. Band model

The band model used consists of a warped heavy band as defined in Eq. (8) of Ref. 1 which permits us to include the nonparabolic effect through the numerical parameter β .

The nonparabolicity of the Ge heavy-mass band is illustrated in Fig. 5(a), where the equilibrium density-of-states effective mass m_h/m_0 calculated in Ref. 20 is reported as a function of thermal energy. The values of β that, according to Eq. (8) of Ref. 1, fit the energy dependence of m_h/m_0 are reported in Fig. 5(b).

The omission of the split-off band is amply justified owing to the large spin-orbit energy Δ and the neglect of the light band, more justified under non-Ohmic conditions,¹² should introduce errors of about 18% to mobility.⁵

B. Scattering mechanisms

Owing to the high purity of the material here used (see Table I), acoustic scattering and non-polar optical scattering mechanisms have been assumed to be the only effective ones.

The scattering probabilities per unit time have been taken, following Eqs. (2)–(4) of Ref. 12, with the parameters reported in Table II. In evaluating the differential and the integrated-scattering prob-

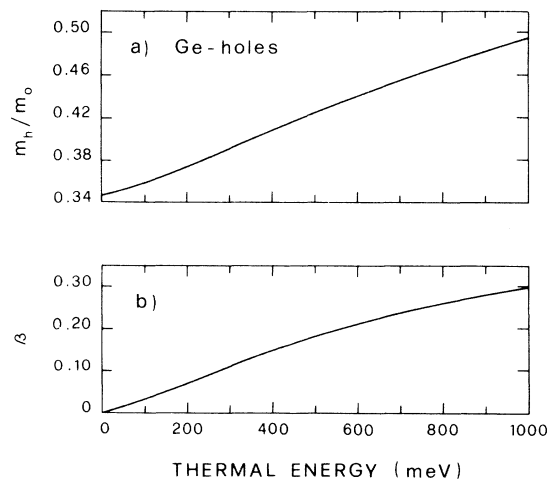


FIG. 5. (a) Equilibrium density-of-states effective mass for the heavy band of Ge as a function of thermal energy; (b) Parameter β as a function of thermal energy (see text).

TABLE II. Constants for Ge.

Quantity	Value	Unit	Reference
A	-13.38	...	21
B	-8.48	...	21
$ C $	13.14	...	21
Δ	0.295	eV	22
ρ	5.32	g/cm^3	23
θ_{op}	430	$^\circ K$	23
s_l	5.4×10^5	cm/sec	23
s_t	3.2×10^5	cm/sec	23
E_1^0	4.6	eV	12
$(D_t K)$	9.0×10^8	eV/cm	12

ability per unit time for acoustic modes, acoustic energy dissipation has been taken to first order in ϵ/ϵ , ϵ and ϵ being the acoustic phonon and the hole energy, respectively, and the Bose-Einstein distribution function has been included in a closely approximated form which avoids the usual energy equipartition and zero-point approximation (see Appendix).

For the sake of completeness, the present deformation potential notation is related to that reported in Ref. 7. Accordingly, the E_1^0 and $(D_t K)$ parameters used here are related to the Ξ_{eff} and d_0 parameters by

$$E_1^0 = \frac{\rho s^2}{C_l} \Xi_{eff}, \quad (D_t K)^2 = \frac{3}{2} \frac{d_0^2}{a_0^2},$$

where $C_l = 1.52 \times 10^{12}$ dyn/cm² is a spherically-averaged elastic coefficient and $a_0 = 5.66 \times 10^{-8}$ cm is the lattice parameter of Ge. The values in this notation agree well with the values of Ref. 7 as reported in Table III. This strongly supports the reliability of the deformation-potential parameters used.

C. Monte Carlo procedure

The transport approach follows a Monte Carlo procedure and, according to the experimental situation, will consider carrier concentration far below degeneracy in the condition where carrier-

TABLE III. Deformation-potential parameters in the formalism of Ref. 7.

d_0 (eV)	Ξ_{eff} (eV)	Reference
41.59	9.24	pw ^a
40.25	8.85 ± 0.4	7

^a pw is present work.

carrier scattering can be neglected. This technique has already been described in Refs. 24–26.

To account for the nonparabolicity of the band, a first approximation was arrived at using the following iterative procedure. First, the different averaged quantities (e.g., $v_d, \langle \epsilon \rangle$) were calculated using the valence-band edge spectrum, i.e., $\beta = 0$. Then, the value $\frac{2}{3} \langle \epsilon \rangle$ so obtained was used to evaluate the corresponding value of β from the plot of Fig. 5(b). With this new value of β , a second run was carried out and the new value of $\frac{2}{3} \langle \epsilon \rangle$ so obtained was used to correct the previous value of β . The process was continued until, still with reference to Fig. 5(b) and within the same simulation, the values of $\frac{2}{3} \langle \epsilon \rangle$ and β were within 10% of each other in energy. Except where otherwise specified, this procedure was used for fields above 10^9 V/cm and/or temperatures above $200^\circ K$. The degree of uncertainty in the computed values is estimated to be at most¹² 5% i.e., at the lowest fields).

IV. THEORETICAL RESULTS AND DISCUSSION

A. Ohmic mobility

The theoretical values of mobility where extrapolated from the v_d/E ratio at the lowest field, and within the limitations of computational uncertainty, had to satisfy the two following conditions: (a) the symmetric condition $v_{d100} = v_{d111}$, and (b) the thermal equilibrium condition $\langle \epsilon \rangle = \frac{3}{2} K_B T$.

Figure 4 compares the theoretical results obtained here with those of previous experiments. The agreement found between theory and experiments is good despite the approximate nature of the model used which, as discussed in the previous section, neglects the light-hole band. It is interesting to note that parabolicity above $200^\circ K$ (dashed line of Fig. 4) increases mobility by about 20% at $300^\circ K$.

B. Drift velocity versus field

The experimental and theoretical drift velocities as a function of temperature and electric field are reported in Fig. 2. The drift velocities obtained in both the $\langle 111 \rangle$ and $\langle 100 \rangle$ directions of the applied field are shown together at a given temperature. Closed and open circles refer to experimental results, continuous and dashed lines to theoretical results. It can be seen that, for fields above about 20 V/cm over the whole temperature range, agreement with experiment is satisfactory. At $T = 8$ and $20^\circ K$ for fields in the range 1–20 V/cm, however, a discrepancy occurs for theoretical calculations do not reproduce anisotropy, and give a lower value for v_d than is found by experiment. In this field

range, calculations afford no evidence of an optical scattering mechanism. Therefore, to clarify theoretical predictions, we performed calculations at 8 °K taking into account acoustic modes only. The results reported in Fig. 6 show that v_d is systematically lower than when both scattering mechanisms (i.e., acoustic and optical) are active. In other words, when an optical scattering mechanism is active in the non-Ohmic region it tends to enhance drift velocity. This effect may be attributed to the strong streaming motion associated with optical phonon emission which causes the distribution function to "peak" in the field direction. These arguments enable one to understand theoretical results, but do not resolve the above discrepancy.

Figure 3 reports the case of $T=77^\circ\text{K}$ for the three directions $\langle 111 \rangle$, $\langle 110 \rangle$, and $\langle 100 \rangle$. As is seen, experiment and theory agree in giving a v_{d110} very close to but greater than v_{d111} .

C. Nonparabolic effects

The net effect of nonparabolicity, tending as it does to decrease both drift velocity and mean energy,¹² improves the agreement between theory and experiment for $E > 10^3$ V/cm over the whole temperature range. As an example, the calculations on v_d performed at $T=77^\circ\text{K}$ are compared in Fig. 7 with experimental values, and it is seen that for field strengths above 10^3 V/cm, nonparabolic effects (continuous lines) consistently make for a better fit than the parabolic model (dashed

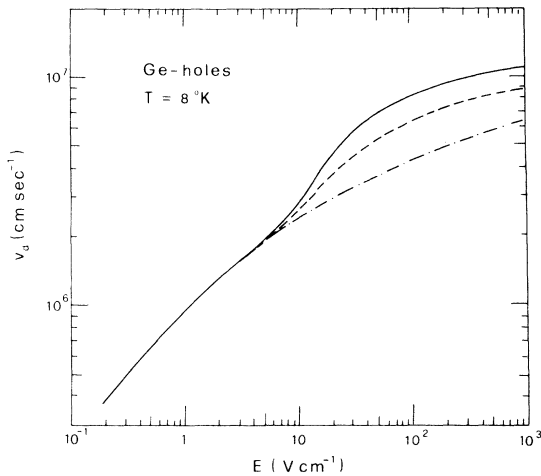


FIG. 6. Hole-drift velocity v_d as a function of electric field at $T=8^\circ\text{K}$. The continuous and dashed curves refer to $\langle 100 \rangle$ and $\langle 111 \rangle$ directions for the case where both optical and acoustic scattering are considered, the dot-dashed curve refers to the case where acoustic scattering only is considered (in this case the values of the $\langle 111 \rangle$ and $\langle 100 \rangle$ directions coincide).

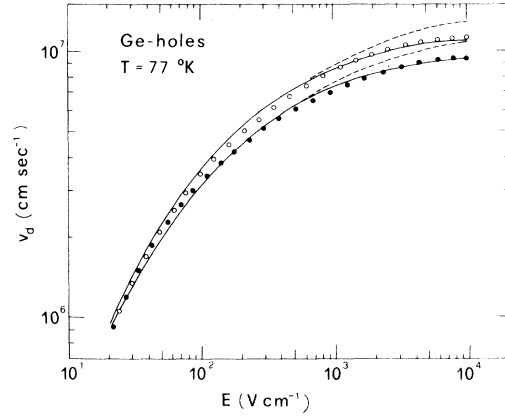


FIG. 7. Hole-drift velocity v_d as a function of electric field at $T=77^\circ\text{K}$. Open and closed circles refer to experimental data obtained with the field parallel to the $\langle 100 \rangle$ and $\langle 111 \rangle$ directions, respectively. Continuous lines indicate the theoretical results obtained for the $\langle 111 \rangle$ and $\langle 100 \rangle$ directions with the inclusion of non-parabolicity effects. Dashed lines refer to the parabolic case with $\beta=0$.

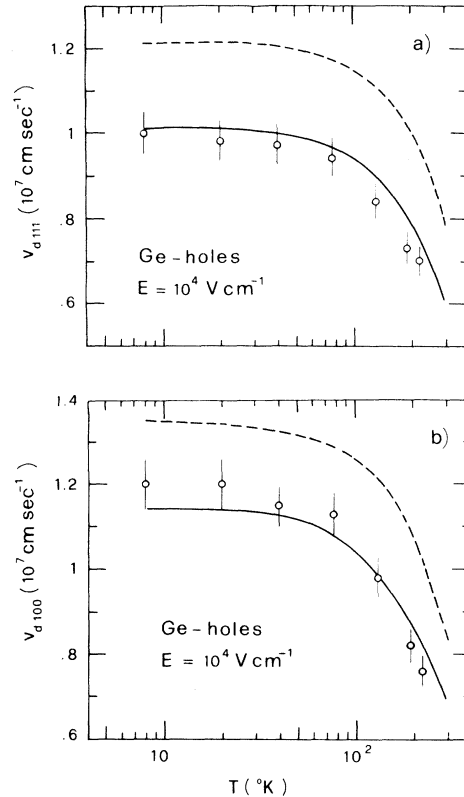


FIG. 8. (a) Drift velocity v_{d111} as a function of temperature for an electric field $E=10^4$ V/cm. \circ , present data. Dashed and continuous lines refer to the respective theoretical calculations in the parabolic case and in the case where nonparabolic effects are taken into account; (b) the same as in (a) for v_{d100} .

lines). In order to clarify this effect, Figs. 8(a) and 8(b) compare the experimental data of v_{d111} and v_{d100} as a function of temperature for $E = 10^4$ V/cm with theoretical calculations. Here, keeping the same constants as in Table II, the dashed line refers to the parabolic model with $\beta = 0$, and the continuous line includes nonparabolic effects. The improved agreement found over the whole temperature range when nonparabolicity is accounted for confirms the importance of this effect at the higher fields, with particular reference to the interpretation of the saturation region of drift velocity.

D. Energy-distribution function

The energy-distribution function $f(\epsilon)$ calculated by Monte Carlo is reported in Figs. 9(a) and 9(b) for different field values at the temperatures indicated. The strong non-Maxwellian shape of the distribution, due to the strong optical-mode scat-

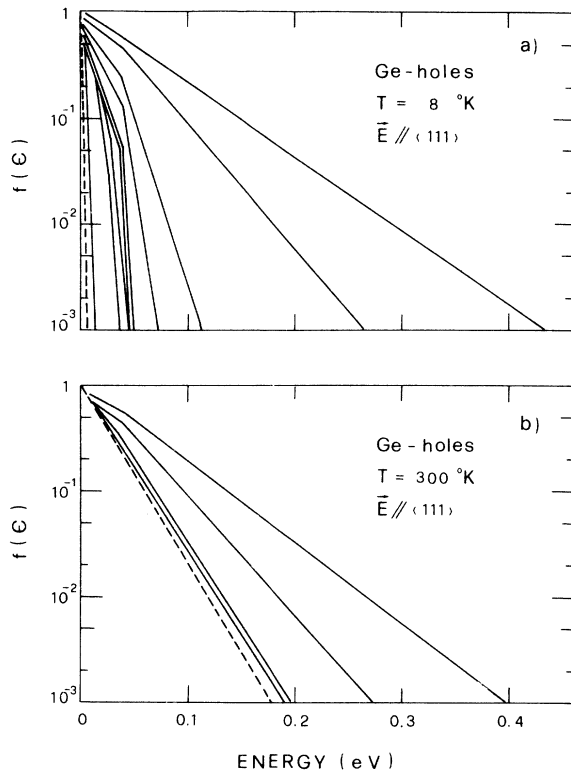


FIG. 9. (a) Energy-distribution functions of holes $f(\epsilon)$ have been obtained at 8 °K with the Monte Carlo calculation (see text). The dashed line refers to zero-field condition and the continuous lines from left to right, to field strengths of 1, 5, 10, 50, 10^2 , 5×10^2 , 10^3 , 5×10^3 , and 10^4 V/cm, respectively. (b) The same as in (a) at 300 °K. The dashed line refers to zero-field condition and the continuous lines from left to right, to field strengths of 5×10^2 , 10^3 , 5×10^3 , and 10^4 V/cm, respectively.

tering, is best observed in the intermediate field range. Since, in these figures, two definite slopes clearly appear both before and after the optical phonon energy, it is argued that the two-temperature Maxwellian approximation²⁷ may be a satisfactory approximation at intermediate and high fields. However, at very low temperatures (e.g., at $T = 8$ °K), and for fields where acoustic dissipation plays the more important role (i.e., $E < 20$ V/cm), this approximation becomes inadequate, since a well-defined distribution slope cannot be assumed.

In Fig. 10 the experimental distribution obtained by Pinson and Bray⁸ is compared with the present theoretical results. In view of the experimental uncertainty, agreement is reasonable. In particular, the theory, which qualitatively reproduces previous results of Budd⁹ and Kurosawa,¹⁰ affords evidence of the anisotropy of the energy-distribution function.

E. Mean-hole energy

The mean-hole energy versus field for E parallel to the $\langle 111 \rangle$ direction, calculated from Monte Carlo, is reported at the indicated temperatures in Fig. 11. At $T = 8$ °K it is seen that the mean energy suddenly increases as field strength increases, as long as the energy balance is governed only by acoustic dissipation (i.e., for $1 \leq E < 20$ V/cm). Then, in the region of intermediate fields (i.e., $20 < E < 10^3$ V/cm), the efficiency of optical phonon emission, in fully dissipating the energy gained by the field, gives rise to a plateau where the mean energy is nearly independent of the field.

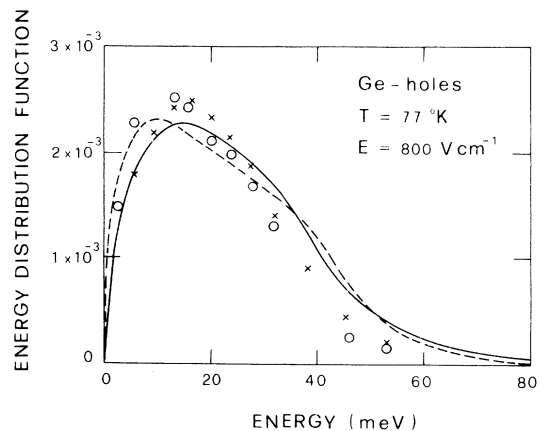


FIG. 10. Comparison between experimental and theoretical energy-distribution function of holes at 77 °K for an electric field $E = 8 \times 10^2$ V/cm. \times , \circ data obtained from Fig. 13 of Pinson and Bray (Ref. 8) corresponding to $E \parallel \langle 100 \rangle$ and $E \parallel \langle 111 \rangle$, respectively. Continuous and dashed lines refer to theoretical results obtained for $E \parallel \langle 100 \rangle$ and $E \parallel \langle 111 \rangle$, respectively.

At the highest fields, the mean energy increases again, as optical phonon emission processes are no longer able to fully dissipate the energy gained by the field. It should be noted that for temperatures above about 77 °K the energy dissipation in the nonlinear response region is always governed by optical-phonon emission.

In the highest-field region the nonparabolic effect is seen to be of great importance in determining mean hole energy; as shown in the insert of Fig. 11, at $E = 10^4$ V/cm, when nonparabolicity is included, mean-hole energy is reduced by about 50% with respect to the parabolic case with $\beta = 0$.

At this field strength, the effective mass used in calculations is about 30% larger than the band-edge value; consequently, it is argued that mean hole energy at high fields is quite sensitive to nonparabolic effects.

Finally, we would point out that the anisotropy of v_d is also reflected in the mean energy. Theoretically, calculations give a consistently higher mean energy for the $\langle 100 \rangle$ than for the $\langle 111 \rangle$ direction. This difference, which increases systematically as field strength increases, is of the order of 10% at the highest field applied.

F. Comparison between Si and Ge data

The similarities of Si and Ge as semiconductors of the same group IV of elements with analogous

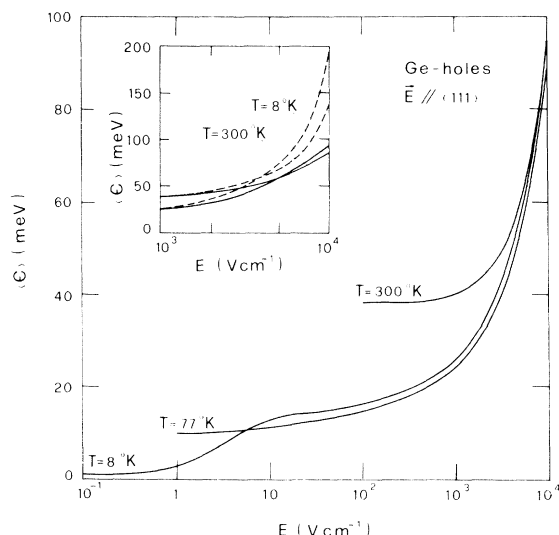


FIG. 11. Mean-hole energy as a function of electric field at different indicated temperatures, obtained with Monte Carlo calculations for the case $E \parallel \langle 111 \rangle$. The inset shows the difference between the case for which nonparabolicity effects are accounted (continuous line) and for the parabolic model with $\beta = 0$ (dashed line) in the region of field strength $E \geq 10^3$ V/cm at the temperatures indicated.

valence-band structure makes interesting a brief comment on the main qualitative differences in the behavior of their hole-drift velocity. By comparing results of Ref. 1 with present ones, it appears that the sharp increases of mobility below about 40 °K and the flattening out of the v_d versus field curve observed in Si at low temperatures and moderate fields does not show up in Ge.

The origin of these differences can be naturally attributed to the larger (about one order of magnitude) spin-orbit energy of Ge than of Si. In fact, it is known^{20,28} that the spin-orbit band is responsible of a strong swelling of the heavy-mass band in the $\langle 110 \rangle$ direction which in turn gives rise to strong nonparabolicity of this band.

In Si, the value of $\Delta = 0.044$ eV causes strong nonparabolic effects at low energies and in a narrow range of them.²⁰ Consequently, an anomalous behavior of mobility at low temperatures and a flattening of the v_d curve at low temperatures and moderate fields is expected to appear (the concomitance of the band swelling and the lowest v_d in the $\langle 110 \rangle$ direction strongly confirms this correlation).

In Ge, the value of $\Delta = 0.295$ eV introduces weak nonparabolic effects at high energies and in an extended range of them.²⁰ Consequently, it is expected a broader correlation between band structure peculiarities and v_d behavior. Accordingly, present results indicate that mobility at room temperature and the saturation drift velocity are affected for about 20% by nonparabolicity.

V. CONCLUSIONS

The hole-drift velocity in Ge has been measured with the time-of-flight technique for a wide range of temperatures $8 \leq T \leq 220$ °K and of fields $1 \leq E \leq 10^4$ V/cm applied parallel to the $\langle 100 \rangle$, $\langle 110 \rangle$, and $\langle 111 \rangle$ directions, and theoretically interpreted following a well-established physical model which accounts for the warping and nonparabolicity effects of the heavy-hole band.

The good agreement found between theory and experiment fully supports the reliability of the model used. In particular, anisotropic effects over the whole range of temperatures and fields have been interpreted as the net effect of band warping.

Nonparabolicity of the heavy-hole band has been found to introduce corrections of the order of 20% on mobility at 300 °K. Furthermore, at the highest fields ($E \geq 10^3$ V/cm), inclusion of nonparabolicity has been found necessary for the interpretation of the saturation region of v_d . A sensitive microscopic parameter of this effect is the mean hole energy, which at the highest fields is half what it is in the parabolic model.

Finally, a theoretical approach which avoids the usual approximation for acoustic scattering (e.g., energy equipartition, zero point, elasticity) and consistently agrees with the classical method (such as the relaxation-time approximation) in the linear-response region, will surely be an effective instrument in dealing with any future problem in this connection.

ACKNOWLEDGMENTS

The authors wish to thank Dr. C. Jacoboni and Dr. P. Lawaetz for their constructive suggestions and stimulating discussions on many aspects of the subject. Professor A. Alberigi Quaranta is acknowledged for his interest and support in the present research. P. Cantoni and M. Bosi are thanked for their assistance in collecting the experimental data. Computer facilities were kindly provided by the Computer Center of the Modena University.

APPENDIX: ACOUSTIC SCATTERING PROBABILITY FOR HOLES

The usual approximations in treating acoustic scattering mechanisms²⁹ are (i) elastic approximation, justified for $\varepsilon/\epsilon \ll 1$; (ii) energy equipartition approximation, justified for $\varepsilon/K_B T \ll 1$. At very low temperatures ($T < 77^\circ\text{K}$) and/or high applied fields both approximations become inadequate. Thus, the hole acoustic scattering in differential as well as in integrated form (as needed in Monte Carlo calculation) is assessed, taking into account the acoustic energy dissipation up to a first order in ε/ϵ , and for the Bose-Einstein distribution function in a closely approximated form. Taking the acoustic phonon in the linear region, the phonon energy involved in carrier scattering between initial \vec{k} and final \vec{k}' states $\varepsilon = \hbar s |\vec{k} - \vec{k}'|$, is well approximated by $\varepsilon \approx \sqrt{2} \hbar s k (1 - \cos\alpha)^{1/2}$, α being the scattering angle.

In order to obtain the integrated scattering probabilities, the integration over the solid angle $d\Omega'$ has been carried out in the "nearly elastic approximation" [i.e., $(\epsilon \pm \varepsilon)^{1/2} \approx \epsilon^{1/2}(1 \pm \varepsilon/2\epsilon)$] and in the "small warping approximation", that is

$$(1 - \beta)a[1 - g(\theta', \varphi')] = \hbar^2/2m_h;$$

$$\int_0^{2\pi} \int_0^\pi d\Omega' \rightarrow 2\pi \int_0^\pi \sin\alpha d\alpha.$$

The former approximation, which is equivalent to the condition $\varepsilon/\epsilon \ll 1$, is well satisfied over the whole range of fields and temperatures in question. The latter approximation is reasonable,

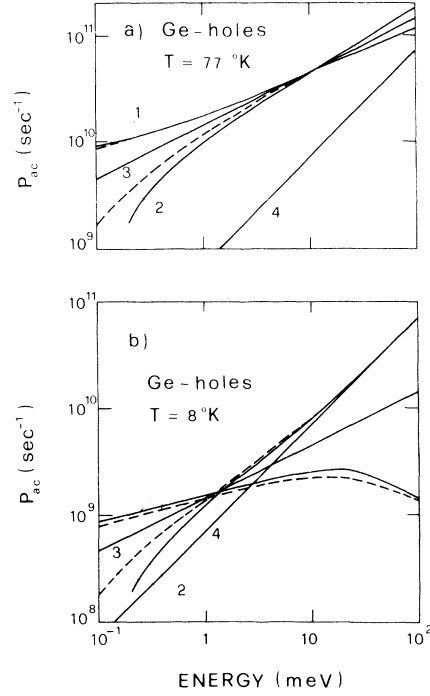


FIG. 12. (a) Integrated acoustic scattering probability as a function of energy for holes in Ge at $T = 77^\circ\text{K}$. Curve 1 refers to absorption processes calculated exactly (dashed line) and in the approximated form (continuous line) given in Eqs. (A1), (A3), (A4). Curve 2 refers to emission processes calculated exactly (dashed line) and in the approximated form given in Eqs. (A2), (A5), (A6). Curve 3 refers to elastic plus energy equipartition approximation. Curve 4 refers to elastic plus zero-point approximation. (b) The same as (a) at $T = 8^\circ\text{K}$.

since it substitutes the density-of-states effective mass for a warping-dependent effective mass.

By approximating the Bose-Einstein function for absorption and emission processes with

$$\frac{1}{e^x - 1} = \begin{cases} 1/x - \frac{1}{2} + \frac{1}{12}x, & x \leq 3, \\ e^{-x}, & x > 3, \end{cases}$$

$$\frac{1}{1 - e^{-x}} = \begin{cases} 1/x + \frac{1}{2} + \frac{1}{12}x, & x \leq 3, \\ 1, & x > 3; \end{cases}$$

the integrated scattering rates for acoustic absorption and emission processes $P_{ac,ab}$ and $P_{ac,em}$ result to be

$$P_{ac,ab} = G\epsilon^{-1/2}[F_1(x_0) + K_B T/\epsilon F_2(x_0)] \quad (\text{A1})$$

$$P_{ac,em} = \begin{cases} G\epsilon^{-1/2}[F_3(x_0) - K_B T/\epsilon F_4(x_0)] & \text{for } \epsilon > 2m_h s^2, \\ 0 & \text{for } \epsilon \leq 2m_h s^2; \end{cases} \quad (A2)$$

with

$$G = E_1^0 m_h^{1/2} (K_B T)^3 / 2^{9/2} \pi \rho s^4 \hbar^4, \quad x_0 = 2m_h^{1/2} s \epsilon^{1/2} / K_B T,$$

and

$$F_1 = \begin{cases} 2x_0^2(1 - \frac{34}{105}\sqrt{2}x_0 + \frac{1}{12}x_0^2) & \text{for } x_0 \leq 3/\sqrt{2}, \\ \frac{1017}{280} + \left(68 - \frac{2358}{x_0^2} + \frac{41931}{x_0^4}\right)e^{-3} - 8e^{-\sqrt{2}x_0} \left(x_0^2 + 4\sqrt{2}x_0 + 28 + \frac{72\sqrt{2}}{x_0} + \frac{252}{x_0^2} + \frac{270\sqrt{2}}{x_0^3} + \frac{270}{x_0^4}\right) & \text{for } x_0 > \frac{3}{\sqrt{2}}, \end{cases} \quad (A3)$$

$$F_2 = \begin{cases} x_0^3 \left(\frac{136\sqrt{2}}{105} - x_0 + \frac{44\sqrt{2}}{315}x_0^2\right) & \text{for } x_0 \leq \frac{3}{\sqrt{2}}, \\ \frac{801}{140} + e^{-3} \left(312 - \frac{13248}{x_0^2} + \frac{300078}{x_0^4}\right) - e^{-\sqrt{2}x_0} \left(8\sqrt{2}x_0^3 + 72x_0^2 + 288\sqrt{2}x_0 + 1824 + \frac{4320\sqrt{2}}{x_0} + \frac{14400}{x_0^2} + \frac{15120\sqrt{2}}{x_0^3} + \frac{15120}{x_0^4}\right) & \text{for } x_0 > \frac{3}{\sqrt{2}}, \end{cases} \quad (A4)$$

$$F_3 = \begin{cases} 2x_0^2 \left(1 + \frac{34\sqrt{2}}{105}x_0 + \frac{x_0^2}{12}\right) & \text{for } x_0 \leq \frac{3}{\sqrt{2}}, \\ \frac{5913}{280} + \frac{136\sqrt{2}}{105}x_0^3 - 9 \left(4 - \frac{162}{5x_0^2} + \frac{729}{7x_0^4}\right) & \text{for } x_0 > \frac{3}{\sqrt{2}}, \end{cases} \quad (A5)$$

$$F_4 = \begin{cases} x_0^3 \left(\frac{136\sqrt{2}}{105} + x_0 + \frac{44\sqrt{2}}{315}x_0^2\right) & \text{for } x_0 \leq \frac{3}{\sqrt{2}}, \\ \frac{6371}{140} + 2x_0^4 - 81 + \frac{729}{x_0^2} - \frac{19683}{8x_0^4} & \text{for } x_0 > \frac{3}{\sqrt{2}}. \end{cases} \quad (A6)$$

The integrated-acoustic scattering probability calculated exactly and with the approximations above introduced, are reported in Fig. 12 together with the usual approximations used in the literature (i.e., energy equipartition and zero point) at $T = 77^\circ\text{K}$ and $T = 8^\circ\text{K}$.

At both temperatures, calculations have shown that acoustic dissipation introduces negligible effects on the integrated acoustic scattering probability. At 77°K energy equipartition affords a good approximation of the total acoustic scattering probability, (i.e., absorption plus emission) over

the whole range of carrier energy, even if the importance of absorption process exceeds that of the emission processes for $\epsilon < \frac{3}{2}K_B T$, while the contrary is true for $\epsilon > \frac{3}{2}K_B T$.

At $T = 8^\circ\text{K}$, and for carrier energy above 10 meV, zero point, instead of energy equipartition, best approximates the physical situation. At this temperature the Ohmic region can still be described by the usual energy equipartition approximation, while the non-Ohmic region needs the more-exact approach.

¹A similar investigation for Si has been reported in G. Ottaviani, L. Reggiani, C. Canali, F. Nava, and A. Alberigi Quaranta, *Phys. Rev. B* **12**, 3318 (1975).

²H. Ehrenreich and A. W. Overhauser, *Phys. Rev.* **104**, 331 (1956).

³H. Ehrenreich and A. W. Overhauser, *Phys. Rev.* **104**, 649 (1956).

⁴D. M. Brown and R. Bray, *Phys. Rev.* **127**, 1593 (1962).

⁵M. Tiersten, *J. Phys. Chem. Solids* **25**, 1151 (1964).

A detailed discussion on the different approximations used in literature can be found in Ref. 6.

⁶M. Costato, G. Gagliani, and L. Reggiani, *Nuovo Cimento Lett.* **4**, 171 (1972).

⁷P. Lawaetz, *Phys. Rev.* **174**, 867 (1968).

⁸R. Bray and W. E. Pinson, *Phys. Rev. Lett.* **11**, 263 (1963); W. E. Pinson and R. Bray, *Phys. Rev.* **136**,

- 1449 (1964).
- ⁹H. Budd, J. Phys. Soc. Jpn. Suppl. 21, 240 (1966); Phys. Rev. 158, 798 (1967).
- ¹⁰T. Kurosawa, J. Phys. Soc. Jpn. Suppl. 21, 424 (1966).
- ¹¹J. P. Nougier and M. Rolland, Phys. Rev. B 8, 5728 (1973).
- ¹²L. Reggiani, J. Phys. Chem. Solids 37, 293 (1976).
- ¹³G. Ottaviani, C. Canali, F. Nava, and J. W. Mayer, J. Appl. Phys. 44, 2917 (1973).
- ¹⁴W. E. Spear, J. Non-Cryst. Solids 1, 197 (1969).
- ¹⁵A. Alberigi Quaranta, C. Jacoboni, and G. Ottaviani, Riv. Nuovo Cimento 1, 445 (1971).
- ¹⁶G. Ottaviani, V. Marrello, J. W. Mayer, M. A. Nicolet, and J. M. Caywood, Appl. Phys. Lett. 20, 323 (1972).
- ¹⁷C. Canali, C. Jacoboni, F. Nava, G. Ottaviani, and A. Alberigi Quaranta, Phys. Rev. B 12, 2265 (1975).
- ¹⁸L. H. De Laet, W. K. Schoenmaekers, H. J. Guislain, and M. Meens, Second Symposium on Sem. Detector for Nuclear Radiation, Munich, 1971 (unpublished).
- ¹⁹D. M. Brown and R. Bray as cited in E. G. S. Paige, in *Progress in Semiconductors*, Vol. 8, edited by A. F. Gibson and R. E. Burgess (Heywood, London, 1964). This book contains a detailed introductory analysis of the hot-hole problem.
- ²⁰G. Gagliani and L. Reggiani, Nuovo Cimento B 30, 207 (1975).
- ²¹J. C. Hensel and K. Suzuchi, Phys. Rev. Lett. 22, 838 (1969).
- ²²A. C. Baynham and E. G. S. Paige, *Proceedings of the Seventh International Conference on the Physics of Semiconductors* (Dunod, Paris, 1964), p. 149.
- ²³E. M. Conwell, in *Solid State Physics*, edited by F. Seitz, D. Turnbull, and H. Ehrenreich (Academic, New York, 1967), Suppl. 9, p. 133.
- ²⁴W. Fawcett, D. A. Boardman, and S. Swain, J. Phys. Chem. Solids 31, 1963 (1970).
- ²⁵P. J. Price, *Proceedings of the International Conference on the Physics of Semiconductors, Moscow, 1968* Paper XV-I (Nauka, Leningrad, 1968).
- ²⁶P. A. Lebowitz, J. Appl. Phys. 44, 1744 (1973).
- ²⁷O. Christensen, Phys. Rev. B 7, 763 (1973).
- ²⁸E. O. Kane, J. Phys. Chem. Solids 1, 82 (1956).
- ²⁹M. Costato and L. Reggiani, Nuovo Cimento Lett. 4, 1179 (1970).